DNA Nanotechnology Hot Paper

Deutsche Ausgabe: DOI: 10.1002/ange.201607050
Internationale Ausgabe: DOI: 10.1002/anie.201607050

3D Framework DNA Origami with Layered Crossovers

Fan Hong, Shuoxing Jiang, Tong Wang, Yan Liu, and Hao Yan**

Abstract: *Designer DNA architectures with nanoscale geometric controls provide a programmable molecular toolbox for engineering complex nanodevices. Scaffolded DNA origami has dramatically improved our ability to design and construct DNA nanostructures with finite size and spatial addressability. Here we report a novel design strategy to engineer multilayered wireframe DNA structures by introducing crossover pairs that connect neighboring layers of DNA double helices. These layered crossovers (LX) allow the scaffold or helper strands to travel through different layers and can control the relative orientation of DNA helices in neighboring layers. Using this design strategy, we successfully constructed four versions of two-layer parallelogram structures with well-defined interlayer angles, a three-layer structure with triangular cavities, and a 9- and 15-layer square lattices. This strategy provides a general route to engineer 3D framework DNA nanostructures with controlled cavities and opportunities to design host–guest networks analogs to those produced with metal organic frameworks.*

Structural DNA nanotechnology provides a programmable route to engineer versatile DNA nanostructures that serve as structural scaffolds in bioengineering, nanometer-scaled electronic engineering, and fabrication.[1] Particularly, DNA origami is a technique that uses hundreds of shorter DNA strands termed helpers, to fold a long single-stranded DNA called the scaffold into desired shapes; this technology has revolutionized our ability to engineer designer nanostructures.[2]

Currently, DNA origami design strategies can be categorized into two major classes: tightly packed and surface wireframe designs. In the tightly packed design, the two-dimensional (2D) structures formed are based on the double crossover (DX) DNA motif[3] that allows antiparallel or parallel alignment of DNA helices in a plane.[4] Mobius stripes,[5] tubes, hollow balls, and flasks[6] are essentially curved surfaces based on multiple DNA helixes arranged in parallel. Similarly, solid block three-dimensional (3D) shapes are achieved by aligning helices in a honeycomb or a square lattice along helical axis, based on six- or four-helix bundle units.[2,7] Surface wireframe designs are realized by linking multi-arm junction units that contain 2 to 12 arms that each contain 1 to 12 helices.[8] The multi-arm junction unit strategy allows nonparallel DNA helix alignment, but the formed structures are either 2D surface structures with various sizes and shaped cavities or 3D polyhedrons that are essentially curved surfaces. A 3D nonparallel alignment such as DNA helices stacked with fixed angles between the neighboring layers to build the 3D framework structures shown in Figure 1 A is not readily achieved by traditional in-plane crossovers or multi-arm junction motifs. Here we present a design strategy that allows the generation of 3D multilayered framework DNA structures with well-controlled geometry using

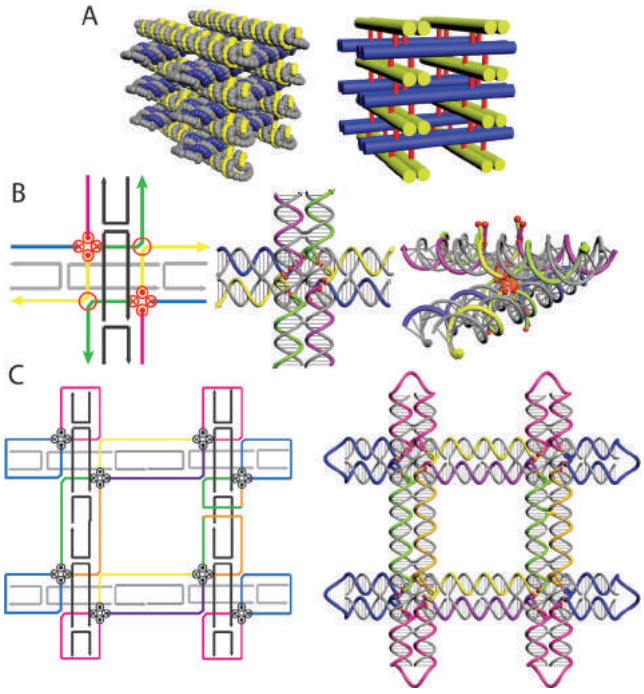

Figure 1. Framework DNA origami structure based on layered-crossover (LX) motifs. A) Left: Helix model of a framework DNA structure with nonparallel DNA helix alignment. Right: the equivalent cylinder model. The short red sticks indicate the crossovers between the layers. B) Line and helix models of a LX motif. Two DX DNA motifs are placed in two layers (vertical on top) connected through a pair of LX (thin red circles) with a controlled relative perpendicular orientation. The potential positions of the LX points on the top and bottom of the motif are also indicated as encircled dots and crosses, respectively. The pair of LXs is located in two opposite DX DNA helices, directing where green and yellow DNA strands travel, which are highlighted in red transparent cylinders. C) A representative double layer of a 2×2 lattice of the LX framework structure. The gray strands are the helpers, and the colored strands represent different portions of the scaffold strand that are joined by single-stranded DNA loops at the DNA helix ends or by scaffold crossovers in the middle of some line segments (middle right DX unit in this example).

[*] F. Hong, Dr. S. Jiang, Prof. Y. Liu, Prof. H. Yan
School of Molecular Science and Biodesign Center for Molecular Design and Biomimetics, The Biodesign Institute
Arizona State University, Tempe, AZ 85287 (USA)
E-mail: yan_liu@asu.edu
hao.yan@asu.edu
Dr. T. Wang
CUNY Advanced Science Research Center, New York, NY (USA)

Supporting information for this article can be found under: http://dx.doi.org/10.1002/anie.201607050.

© 2016 Wiley-VCH Verlag GmbH & Co. KGaA, Weinheim

novel layered-crossover (LX) motifs where each line segment is based on the DX DNA motif (Figure 1 B).

The LX motifs are introduced to connect neighboring DNA helices in different layers, so both the helper and scaffold strands can travel between layers to form the designed framework shapes. These LX motifs are depicted as short red sticks in the cylinder model shown in Figure 1 A. A typical LX motif in a two-layer unit is shown in Figure 1 B, in both line and helix models. The two horizontal helices are beneath the two vertical helices, and each contains a DX motif. A pair of LXs (highlighted in the red circles) are located in the two helices opposite the two DX motifs, directing the green and yellow DNA strands to travel between the layers (Figure 1 B).

The two-layer LX units can be directly joined in the ends of DNA helices (as shown in Figure 1 C) to form a 2D lattice; they can also be connected between layers through LX connections located at the top and bottom of two layers (encircled dots and crosses pointing up and down, respectively) into multilayer wireframes. Connecting these units end to end and top to bottom produces a 3D framework lattice structure. Figure 1 C shows the routes of the DNA strands. The colored lines represent different segments of the long single-stranded scaffold DNA that travels through the layers of the structure. The gray strands represent the short helper strands. The colored strands are joined at the helix ends by small loops and between the layers by LXs. Finally, some proper scaffold crossovers are placed in selected line segments to make the scaffold a single-stranded loop that passes twice through each line segment in different layers. Either the helper (H) or scaffold (S) strands can be directed to travel between the layers at the LX points (see Figure S2 in the Supporting Information). In addition, the two-layered unit connected by LX has four arms specified as north (N), south (S), west (W), and east (E). Starting from the N arm, the strands traveling between the layers can go in two ways: NW or NE. Thus, we can produce four different LX motifs: HNW, HNE, SNW, and SNE (Figure S2).

The positions of the DX points should be adjacent to each other when the two helices are antiparallel to minimize structural distortion in the traditional DX molecule. Similarly, the LX points should be located on the most top or bottom region of DNA helices to minimize the distance of the two DNA helices between layers. A simple geometric model is applied to identify potential LX positions and estimate the relative orientations of DNA helices in the neighboring layers. The coordinates of phosphates of each nucleotide (nt) in the *xyz*-axis are based on the structural parameters of B-type DNA and DX DNA molecules. The detailed geometric model is described in the Supporting Information (Figures S3–4). The *z*-coordinate of the center of the helix is defined as 0, and a threshold of 0.85 nm at the *z*-axis is set to screen potential LX positions on the top of the DX. For example, if the *z* coordinate of a phosphate is >0.85 nm, it means it is located on the top of a helix structure and can serve as a crossover point that directs the strand traveling to the upper layer. This method was used to identify all the potential LX positions provided by either scaffold or helpers in a six-turn DX unit (Figures S4–7). Using different combinations of the possible LX points identified from the geometric model, the angles of DNA helices in neighboring layer can be calculated. For example, the combinations of 1-6, 2-5, 3-4 and 4-3 give discrete angle values of 16, 25, 61, and 86° when only the acute angle is considered. Figure 2 A shows one of the two-layer units with a predicted angle of 86° between the layers that uses the HNW LX motif (the remaining structure motifs are shown in Figure S7). A series of two-layered parallelogram constructs with different angles were designed by connecting 25 of these two-layer units (5×5; Figure 2 C and Figures S9–12).

When the HNW LX motif is used, the scaffold strand is continuous within each helix (Figure 2 A). Figure S9 illustrates the stepwise scaffold routing. The ends of the helices

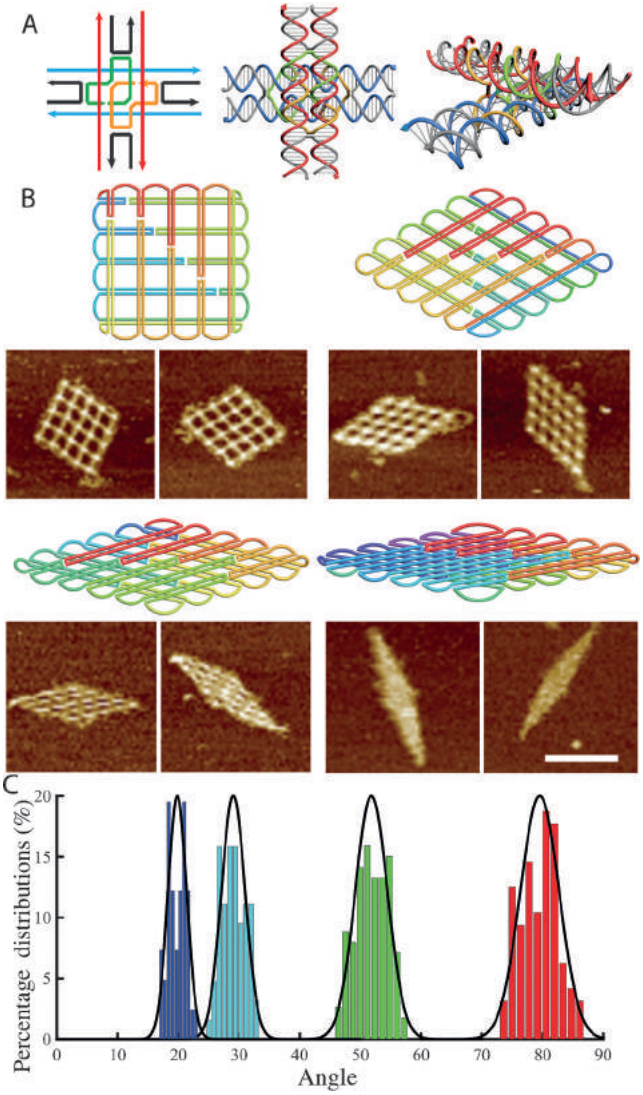

Figure 2. Two-layered constructs of 5×5 parallelogram lattices with various angles. A) The line and helix models of a two-layer unit linked by two helper layered crossovers (HNW) with a predicted angle of about 85° between the DNA helixes in both layers. B) Scaffold routing pathways and representative AFM images of the four angle distributions observed in individual particles. Scale bar = 100 nm. C) Histograms of angle distributions observed in individual particles. The mean corner angles were determined to be $20\pm2°$ ($n=41$), $29\pm2°$ ($n=64$), $52\pm3°$ ($n=113$), and $80\pm3°$ ($n=96$). A single-peak Gaussian function was used to fit the histograms.

© 2016 Wiley-VCH Verlag GmbH & Co. KGaA, Weinheim

are first connected by single-stranded loops of proper lengths, then scaffold crossovers are placed at selected locations. This allows the scaffold strand to form a single loop so that a typical single-stranded M13 DNA can be used as the scaffold, with rainbow coloring representing the routing sequence (Figure 2B). Unpaired single-stranded loops on the edges of the structure can prevent π–π stacking along blunt-ends of DNA helices. For this group of four different two-layered constructs with different interlayer angles, 6752 of the 7249 nt in the scaffold strand were used. The unused scaffold strand (ca. 500 nt) remains looped at one corner of the structure. The Successful formation was confirmed with atomic force microscopy (AFM; Figure 2D, with additional images in Figures S30–33). Imaging showed that the majority of structures formed the designed shapes. The high formation yields were verified with native agarose gel electrophoresis (Figures S16–19). The relative bright spots located in the intersections in the AFM images indicate the presence of two layers. The repeating distance between the bright spots is about 15 nm, which matches the designed length of four DNA helical turns in each line segment. The formation and melting processes of these structures were observed in the presence of SYBR Green I using qPCR with slow cooling and heating (ca. 0.1 °C min^{-1}, Figures S23–26). The mean melting temperature of these four structures was 61 ± 1°. The distribution of angles between the DNA helices in the two layers was measured on AFM images by statistical analysis.

The values were 80 ± 3, 52 ± 3, 29 ± 2, and 20 ± 2° for the four different constructs. The narrow range of angle distributions (2–3° of standard deviation) demonstrates the robustness and precision of controlling relative DNA helix orientation in the neighboring layers. These experimentally measured angles are close to the predicted values from the geometric model (86, 61, 25, and 16°). The small discrepancy may be attributed to the assumption of the geometric model that each DX line segment is rigid and cylindrical. In reality, the portions of the two DNA helices between the two crossovers actually bend outward due to electrostatic repulsions,[9] which was not considered in the simple geometric model. Nevertheless, this model still provides rational guidance to structure design, with the angles produced matching those predicted.

We next designed a three-layered structure using scaffold LX with a predicated angle of about 60°. The repeating unit of the structure is shown in Figure 3A in both line and helix models, with the scaffold strand (blue and green) traveling through the three layers at each intersection via LX twice. From the top, the scaffold routing (Figure 3B) shows a truncated triangle with triangular cavities. AFM images (Figure 3C) confirmed successful structure formation with triangular cavities with bright spots at the intersections. Additional AFM images can be found in Figure S36.

A 9-layered 3 × 3 lattice and a 15-layered 2 × 2 lattice were also constructed (Figure 4). To directly reveal the native 3D feature of the assembled structures, the samples were imaged with cryoelectron microscopy (cryoEM), and individual particles could easily be identified in the raw images (Figure 4A & C). Particle morphology resembles the 2D projections of the lattice structure from the side or top. A single

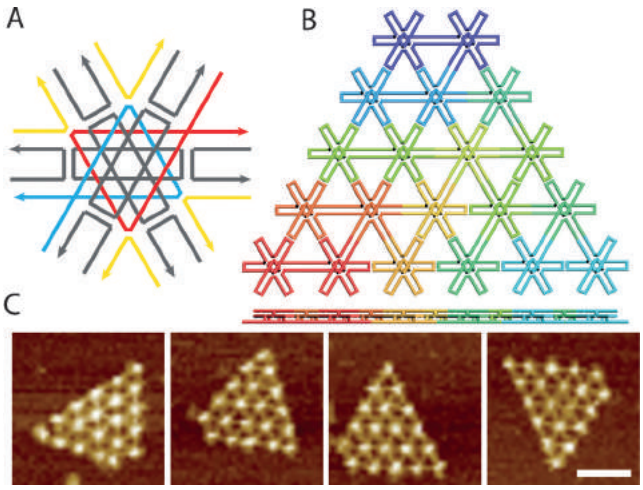

Figure 3. A three-layered construct of framework structure with triangular cavities. A) The line and helix models of a three-layer unit. Scaffold LXs are introduced to control the relative DNA helix orientation in neighboring layers with a 60° angle (e.g., the yellow strands transverse between two layers, while the green and blue strands transverse through all three layers). B,C) Scaffold folding pathway and representative AFM images of the three-layered truncated triangle structures. Scale bar = 50 nm.

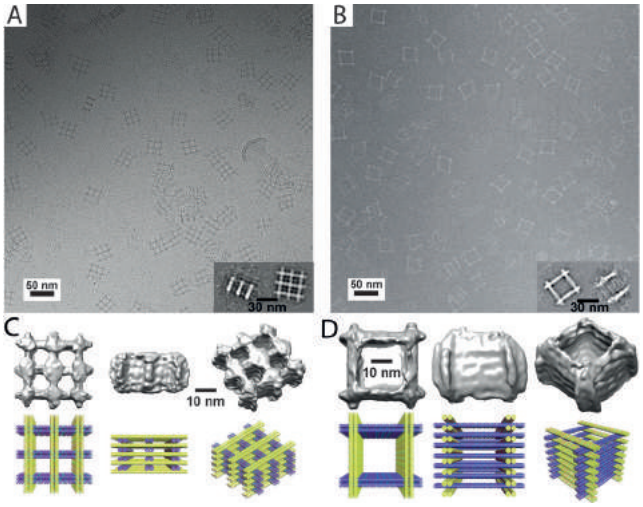

Figure 4. A 9-layered 3 × 3 latticed framework structure and 15-layered 2 × 2 framework structure. A,C) The raw cryoEM micrographs of the two structures and their class averages. B,D) Three views of the 3D structural model reconstructed from the observed particles in cryoEM images and the corresponding views of the cylinder models.

particle reconstruction technique was used to solve the structure of the framed complex. The detailed reconstruction procedure can be found in the Supporting Information. The reconstructed 3D particle confirms that the structures assembled match the designed models (Figure 4B & D). Two-fold symmetries in the top, front, and side views were identified. The measured dimensions of the structures were approximately 40 nm wide and 20 nm high for the 9-layer 3 × 3 lattice structure and 40 nm wide and 40 nm high for the 15-layer 2 × 2 lattice structure. The smaller cavities (ca. 2–2.5 nm wide) expected on the side views were not clearly visible due to the

© 2016 Wiley-VCH Verlag GmbH & Co. KGaA, Weinheim

limited resolution (ca. 2.4 nm), but a wavy surface indicated their existence.

The formation of 3D compact solid origami structures with parallel DNA helix alignment usually requires relatively long annealing times (> 30 h) to avoid kinetic traps, as well as high magnesium (Mg^{2+}) concentrations in the buffer (about 15–30 mM) to suppress electrostatic repulsion of the negatively charged phosphate backbones between adjacent helices.[7a] The structure formation of the framework 3D structure was tested in a set of buffer with a Mg^{2+} concentration titrated from 0 to 20 mM. The agarose gel images shown in Figures S21 and S22 show sharp bands starting from the lanes with 8 or 10 mM. The samples formed in 12 mM Mg^{2+} buffer were imaged with cryoEM (Figures S35 and S36), and the results indicated high formation yield. Therefore, compared with solid structures, our framework 3D DNA structures are more readily formed because of less electrostatic repulsion between the DNA helices and greater accessibility for helper stands to be incorporated into the growing structures.

In summary, we demonstrated a reliable design method for engineering 3D framework DNA origami structures with various pore shapes and sizes by using LX motifs. These motifs allow nonparallel alignment of DNA helices in a layer-by-layer fashion with predictable angles and geometries. Like DX molecules and multi-arm junction motifs, the LX motif enriches the structural DNA nanotechnology toolbox. Our results show that the LX motif is useful for generating DNA origami with finite sizes, and it could be applied to the tile-based self-assembly for the growth of 2D or 3D crystals. Unlike traditional multi-arm junction tile with no out-of-plane extension that yields a single 2-nm thick layer,[10] LX tiles can build 2D DNA crystals with controllable geometries and depths. The porous feature of framework DNA nanostructures also offers new opportunities for several applications. For example, DNA origami can serve as a template to guide the synthesis and control the ultimate geometry of heteronanomaterials.[11] Framework DNA structures could serve as templates to synthesize porous nanomaterials with novel properties, such as catalysis[12] or light harvesting.[13] Furthermore, framework DNA structures can serve as scaffolds to organize enzymatic reactions in a 3D periodic style. Reaction efficiency has already been improved by using 2D DNA origami or DNA origami containers to localize enzymatic reactions.[14] The Diffusion of reaction intermediates from one enzyme to another is a crucial step for efficient enzymatic reaction cascades. In 1D or 2D DNA structures, intermediates can diffuse away to the bulk solution, limiting coupling efficiency. Unlike traditional origami structures with only one surface available for enzyme attachment, the framework origami structure engineered here can organize enzymes in a 3D latticed structure. The porous features of framed structures allow rapid diffusion of the intermediates within the structure and reduces their escape into the local reaction environment. Overall, the framework DNA structure based on the LX motif provides new opportunities for DNA structures in a wide range of applications.

Acknowledgements

This work was supported by grants from National Science Foundation, the Army Research Office and Office of Naval Research to H.Y. and Y.L.

Keywords: DNA nanotechnology · DNA origami structures · framework structures · molecular programming · self-assembly

How to cite: *Angew. Chem. Int. Ed.* **2016**, *55*, 12832–12835
Angew. Chem. **2016**, *128*, 13024–13027

[1] a) F. A. Aldaye, A. L. Palmer, H. F. Sleiman, *Science* **2008**, *321*, 1795–1799; b) A. V. Pinheiro, D. Han, W. M. Shih, H. Yan, *Nat. Nanotechnol.* **2011**, *6*, 763–772; c) N. C. Seeman, *Nature* **2003**, *421*, 427–431.

[2] H. Dietz, S. M. Douglas, W. M. Shih, *Science* **2009**, *325*, 725–730.

[3] T. J. Fu, N. C. Seeman, *Biochemistry* **1993**, *32*, 3211–3220.

[4] a) E. S. Andersen, M. Dong, M. M. Nielsen, K. Jahn, R. Subramani, W. Mamdouh, M. M. Golas, B. Sander, H. Stark, C. L. Oliveira, J. S. Pedersen, V. Birkedal, F. Besenbacher, K. V. Gothelf, J. Kjems, *Nature* **2009**, *459*, 73–76; b) D. Han, S. Jiang, A. Samanta, Y. Liu, H. Yan, *Angew. Chem. Int. Ed.* **2013**, *52*, 9031–9034; *Angew. Chem.* **2013**, *125*, 9201–9204; c) P. W. K. Rothemund, *Nature* **2006**, *440*, 297–302.

[5] D. Han, S. Pal, Y. Liu, H. Yan, *Nat. Nanotechnol.* **2010**, *5*, 712–717.

[6] D. Han, S. Pal, J. Nangreave, Z. Deng, Y. Liu, H. Yan, *Science* **2011**, *332*, 342–346.

[7] a) S. M. Douglas, H. Dietz, T. Liedl, B. Högberg, F. Graf, W. M. Shih, *Nature* **2009**, *459*, 414–418; b) Y. Ke, S. M. Douglas, M. Liu, J. Sharma, A. Cheng, A. Leung, Y. Liu, W. M. Shih, H. Yan, *J. Am. Chem. Soc.* **2009**, *131*, 15903–15908; c) Y. Ke, N. V. Voigt, K. V. Gothelf, W. M. Shih, *J. Am. Chem. Soc.* **2012**, *134*, 1770–1774.

[8] a) E. Benson, A. Mohammed, J. Gardell, S. Masich, E. Czeizler, P. Orponen, B. Högberg, *Nature* **2015**, *523*, 441–444; b) D. Han, S. Pal, Y. Yang, S. Jiang, J. Nangreave, Y. Liu, H. Yan, *Science* **2013**, *339*, 1412–1415; c) S. S. Simmel, P. C. Nickels, T. Liedl, *Acc. Chem. Res.* **2014**, *47*, 1691–1699; d) F. Zhang, S. Jiang, S. Wu, Y. Li, C. Mao, Y. Liu, H. Yan, *Nat. Nanotechnol.* **2015**, *10*, 779–784; e) M. Matthies, N. P. Agarwal, T. L. Schmidt, *Nano Lett.* **2016**, *16*, 2108–2113.

[9] X.-c. Bai, T. G. Martin, S. H. Scheres, H. Dietz, *Proc. Natl. Acad. Sci. USA* **2012**, *109*, 20012–20017.

[10] a) Y. He, Y. Chen, H. Liu, A. E. Ribbe, C. Mao, *J. Am. Chem. Soc.* **2005**, *127*, 12202–12203; b) Y. He, Y. Tian, A. E. Ribbe, C. Mao, *J. Am. Chem. Soc.* **2006**, *128*, 15978–15979; c) H. Yan, S. H. Park, G. Finkelstein, J. H. Reif, T. H. LaBean, *Science* **2003**, *301*, 1882–1884.

[11] a) Z. Jin, W. Sun, Y. Ke, C.-J. Shih, G. L. Paulus, Q. H. Wang, B. Mu, P. Yin, M. S. Strano, *Nat. Commun.* **2013**, *4*, 1663; b) W. Sun, E. Boulais, Y. Hakobyan, W. L. Wang, A. Guan, M. Bathe, P. Yin, *Science* **2014**, *346*, 1258361.

[12] C. Chen, Y. Kang, Z. Huo, Z. Zhu, W. Huang, H. L. Xin, J. D. Snyder, D. Li, J. A. Herron, M. Mavrikakis, *Science* **2014**, *343*, 1339–1343.

[13] P. K. Dutta, R. Varghese, J. Nangreave, S. Lin, H. Yan, Y. Liu, *J. Am. Chem. Soc.* **2011**, *133*, 11985–11993.

[14] a) J. Fu, M. Liu, Y. Liu, N. W. Woodbury, H. Yan, *J. Am. Chem. Soc.* **2012**, *134*, 5516–5519; b) J. Fu, Y. R. Yang, A. Johnson-Buck, M. Liu, Y. Liu, N. G. Walter, N. W. Woodbury, H. Yan, *Nat. Nanotechnol.* **2014**, *9*, 531–536.

Received: July 20, 2016
Revised: August 31, 2016
Published online: September 15, 2016

© 2016 Wiley-VCH Verlag GmbH & Co. KGaA, Weinheim